Available online at www.sciencedirect.com
SCIENCE DIRECT®
Earth and Planetary Science Letters 248 (2006) 43–53
EPSL
www.elsevier.com/locate/epsl

Structural record of an oblique impact

Dirk Scherler [a,*], Thomas Kenkmann [b], Andreas Jahn [b]

[a] Universität Potsdam, Institut für Geowissenschaften, Postfach 601553, D-14415 Potsdam, Germany
[b] Humboldt-Universität zu Berlin, Museum für Naturkunde, Institut für Mineralogie, Invalidenstrasse 43, D-10115 Berlin, Germany

Received 14 December 2005; received in revised form 28 April 2006; accepted 1 May 2006
Available online 7 July 2006
Editor: R.W. Carlson

Abstract

Most impactors strike their target at an oblique angle. The common criterion for identifying craters formed by an oblique impact is the pattern of the ejecta blanket. On Earth, however, ejecta blankets are rarely preserved and other morphological, structural or geophysical criteria are needed. Here, we present structural details from the central uplift of the Upheaval Dome impact structure that are diagnostic of the kinematics during crater collapse and central uplift formation. A characteristic imbrication of thrust slices towards the SE, the pattern of strata orientation within the central uplift, dominant radial faults that accommodated NW–SE shortening and an elliptical bedding outline indicate that the displacement field during crater collapse has not been axial symmetric. Instead, an additional lateral component, roughly towards the SE, is preserved in the internal structure of the central uplift. The structural asymmetries are largest in the core of the central uplift and disappear outwards, thereby preserving the large-scale circular shape of the main structural elements (rim monocline, ring syncline). Comparison with numerical models of oblique impacts suggests that the additional lateral displacement component reflects a downrange material transport during the initial stages of central uplift formation. Similar patterns are identified in other impact structures and may serve as general criteria for identifying the impact direction of deeply eroded impact structures in sedimentary targets.

Keywords: impact crater; oblique impact; impact angle; crater collapse; central uplift; Upheaval Dome

1. Introduction

The importance of meteorite impacts in shaping the surfaces of planetary bodies is now widely recognized (e.g., [1]). The product of an impact is a usually circular scar, despite the fact that half of all impacts strike their targets at an angle between 30° and 60° [2,3]. It is known from laboratory-scale experiments that elliptical craters require impact angles as low as ~5–10° [4,5], which occur as rare as near vertical impacts [3]. More sensitive to the impact angle is the distribution of the ejecta blanket, which first becomes asymmetric and with decreasing angle develops a forbidden zone in the uprange and then downrange direction at angles of less than ~45° [4,6]. Experimental and numerical studies have shown that the distribution of peak shock pressures within the target is asymmetrical in the case of oblique impacts [7], and therefore may exert control on the amount of climatically active gases released from upper crustal rocks to the atmosphere [8], as proposed for the Chicxulub impact event [9]. Deviation of the impact angle from vertical has also been suspected to be responsible for the launch of Martian meteorites [11–13].

* Corresponding author. Tel.: +49 331 977 5788; fax: +49 331 977 5700.
E-mail address: dirk@geo.uni-potsdam.de (D. Scherler).

0012-821X/$ - see front matter © 2006 Elsevier B.V. All rights reserved.
doi:10.1016/j.epsl.2006.05.002

The common criterion for identifying craters formed by an oblique impact is the pattern of the ejecta blanket. On Earth, however, ejecta blankets are rarely preserved and morphological, structural, geophysical as well as depositional criteria, including tektite distribution, have been used to infer an oblique impact (as has been done for the Chicxulub [9,10], Manson [14], Spider [15], Ries and Steinheim [16], Upheaval Dome [17], Mjölnir [18] and Lockne [19] impact structures). However, the significance of such criteria in predicting impact angle or direction is a matter of debate. For example, based on gravity and aeromagnetic data of the Chicxulub impact structure, Schultz and D'Hondt [9] and Hildebrand et al. [10] inferred a different impact direction (from SE vs. SW) and angle (20–30° vs. 60° from horizontal), though both author teams were basically using criteria proposed by [14]. It is important to highlight that it is not yet known whether there is an influence of the impact angle on the displacement field during the collapse of large transient cavities, and thus, the final crater as required for all craters on earth larger than 2–4 km (depending on target lithology [20]), i.e. all cited examples. For most impact angles, the shape of the final crater is controlled by its size. At the aforementioned critical diameter, simple bowl-shaped craters become gravitationally unstable and collapse to form complex craters, which possess a flat floor and terraced rim [20]. During collapse, the crater floor rises to form a central uplift that may or may not be visible as a central peak, or as a peak ring at yet larger diameters. Schultz and Anderson [14] proposed, that (1) enhanced rim/wall collapse in the uprange direction, (2) an uprange offset of the central uplift, combined with (3) a downrange breaching, and (4) a large central uplift diameter relative to crater diameter, are structural features in complex craters related to impact angle and direction. However, Ekholm and Melosh [21] studied Venusian craters and concluded that (2) and (4) are statistically unwarranted criteria for assessing an oblique impact. While observations from Venus support the first criterion [22], the third lacks enough examples to be supported or disproved. Recently, Shuvalov [23] and Shuvalov and Dypvik [24] observed in three-dimensional numerical simulations of oblique impacts that the early stage of crater collapse is characterized by an asymmetrically shaped transient cavity and an uprange offset of the rising central uplift. Yet, during ongoing collapse of the transient cavity, the rising uplift migrates downrange and therefore eliminates the initial asymmetry.

Our working hypothesis is that the internal geometry of the central uplift can yield information about the symmetry or asymmetry of the subsurface crater flow field during central uplift formation, and hence, allows to infer the impact direction. Excellent exposure of originally almost flat lying sedimentary rocks at the deeply eroded Upheaval Dome impact structure, in SE Utah, allow a detailed picture to be gained of the internal structure of a central uplift and the kinematics of its formation. The results of our field mapping in the innermost part revealed a systematic arrangement of structural features, indicative of a lateral displacement component in addition to the axial-symmetric displacement field during crater collapse. We propose that this lateral component reflects a shift in the onset of crater collapse and the migration of the uplifting crater floor downrange.

2. Study area

The Upheaval Dome impact structure is situated near the confluence of the Colorado and Green River in Canyonlands National Park on the Colorado Plateau in SE Utah (Fig. 1). It lies on the gentle (1°) NNW-dipping southwestern limb of the NW-trending Grays Pasture syncline [25]. The outer limit of the structure is defined by a rim monocline of ~5.2 km in diameter. A ring syncline delineates the boundary of the central uplift at a distance of ~1.8 km from the center of the structure, which is located at approximately 38°26′14″N, 109°55′43″W. The outcropping units range from the Permian White Rim Sandstone (Cutler Group) in the topographically depressed center of the dome-shaped central uplift, to the erosively capped Jurassic Navajo Sandstone (Glenn Canyon Group) in the ring syncline (Fig. 1).

2.1. Structural inventory of the central uplift

A central uplift is the result of in-and upward-directed movement of rocks during crater collapse and their crowding in the center. At Upheaval Dome, inward displacement has taken place on low angle listric normal faults that are exposed near the rim of the structure [26]. The radial convergent material flow resulted in concentric shortening and the formation of radial transpression ridges [27]. These are manifested as radial outwards plunging folds in the thick-bedded and massive Jurassic Wingate and Navajo Sandstone [28]. The layered Kayenta Formation in between mimics these folds, but also shows numerous faults that accommodated dominantly radial and subordinate concentric displacements [29]. In contrast, the majority of the faults in the thin-bedded Triassic Chinle and Moenkopi Formations, and particularly those with the largest offsets, are arranged in a (sub)radial fashion (Fig. 2A). Displacement on these

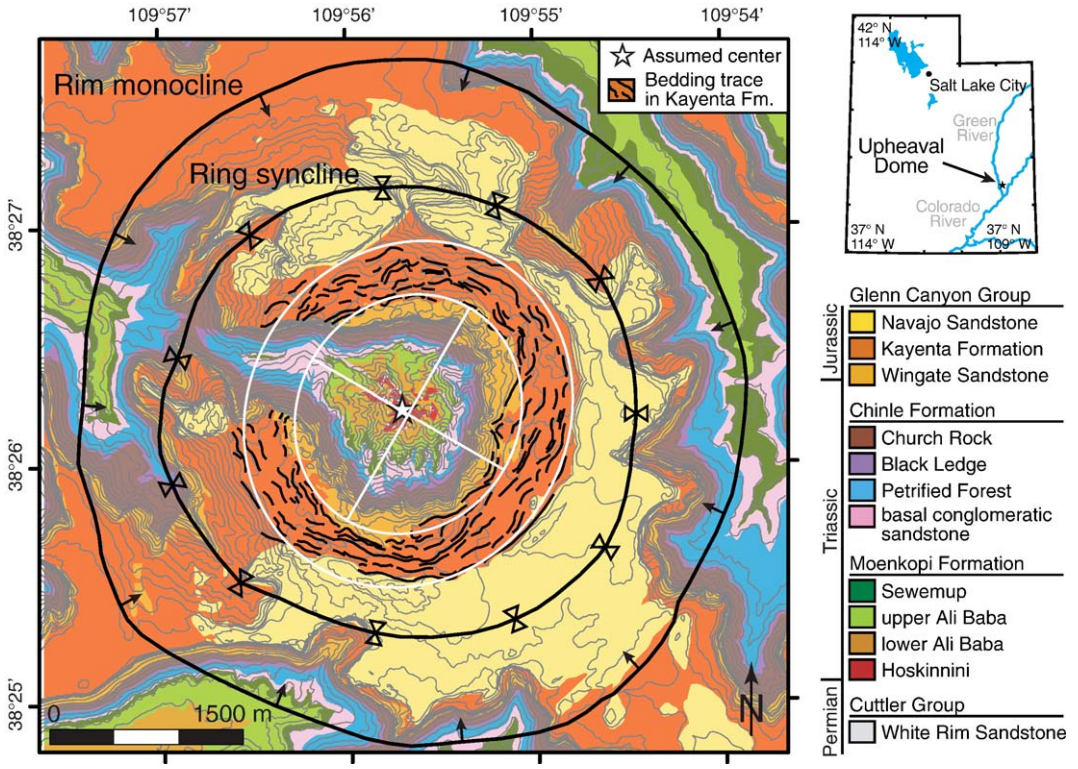

Fig. 1. Geological map of the Upheaval Dome impact structure. The trace of the rim monocline and ring syncline are averaged from the traces given by [28,29] and corrected for jumps in distance from the center due to topography. The white ellipses highlight the prevailing strike directions of the beds within the Kayenta Formation and the inner lines mark the short (NW–SE) and long (SW–NE) axis. Geological map compiled from Kriens et al. (1999) and own mapping results as delineated in Fig. 2A.

faults increases towards the center and, therefore, invokes the analogy of a camera diaphragm as a mechanism accommodating concentric shortening [29]. Fault density also increases and many of the large faults end up at clastic dikes of the White Rim Sandstone [30]. Close to the center, throws of usually around 50 m and rarely more than 100 m can be estimated by the juxtaposition of different stratigraphic units (Fig. 2B). By comparing the heights of individual layers that crop out near the center of the central uplift as well as beyond the crater, a structural uplift of ~200 m can be estimated.

3. Methods

A detailed mapping campaign was conducted in the innermost part of the central uplift, covering the units stratigraphically below the Black Ledge member of the Chinle Formation. In order to combine the results with the geological map by [28], the same stratigraphic units were discriminated, though slight deviations regarding the definition of the lithological boundaries occur for some units. Only those faults with offsets of more than 2 m were taken into account. The degree of detail varies due to difficult access of areas with steep slopes. Bedding orientation was taken at about 1100 locations during the mapping. The data was compiled in a GIS-model with digital elevation data (10 m resolution) provided by the U.S. Geological Survey. A complete map and a three-dimensional model of the central uplift can be found in [17]. Thematic maps were created using ArcGIS 8 and the 3D Analyst extension by ESRI. Mapping of bedding traces within the Kayenta Formation was done using high-resolution aerial and satellite images. Digitized and orthorectified aerial photographs (digital orthoquadrangles) from the USGS with a spatial resolution of ~1 m were acquired from Terraserver-USA. In addition, we acquired a natural colored Quickbird satellite image (non-rectified) with a resolution of ~2.5 m from the sample library of Digitalglobe in order to assess correct mapping of the multicolored beds.

4. Results

In the following, we describe five structural features that are indicative for a non-axial-symmetric flow field during central uplift formation at Upheaval Dome.

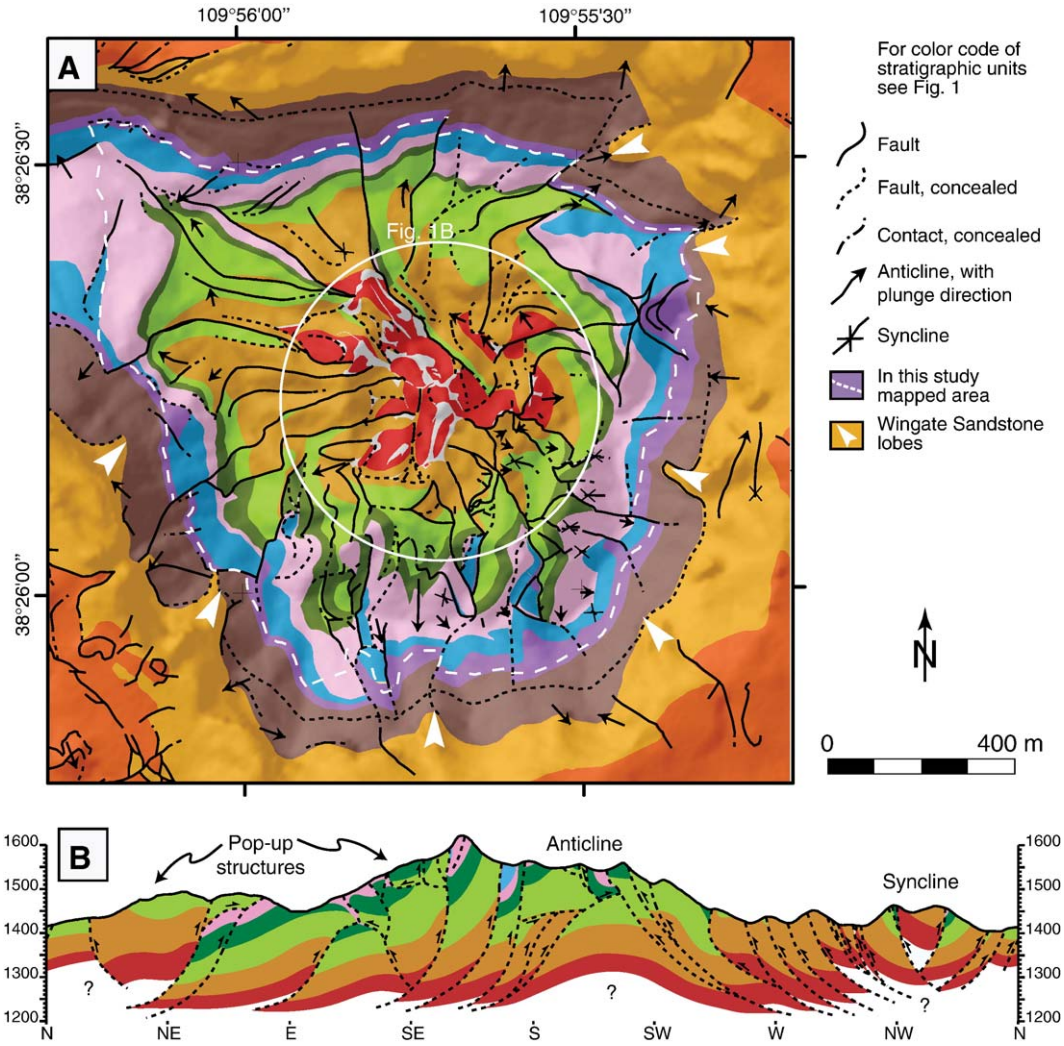

Fig. 2. (A) Geological map of the central uplift of Upheaval Dome. The small white circle in the center gives the location of the circular cross section in B. (B) Circular cross section through the innermost part of the central uplift. Thickening of units is usually due to dip of strata out of the plane of section. Structural evolution at depth between E and SW, where section crosses the ridge line of topographically elevated part, is projected from further inward.

4.1. Central imbrication structure

The arrangement of the major radial faults within the Triassic rocks systematically departs from an idealized circumferential imbricate structure, such as a camera diaphragm. Beginning at a syncline in the NNW, the fault bound slices are imbricated towards an anticline in the S (Fig. 2A). While the faults in the northeastern sector mostly dip in a clockwise direction (with respect to the center), those in the southwestern sector dip in a counterclockwise direction (Fig. 3A). Therefore, most of the faults are W- to N-dipping, indicating top-to-the E to S thrusting. Moreover, at equal distance to the center, the structural elevation is highest in the syncline and drops to both sides (Fig. 2B). This suggests that the structurally most elevated part of the central uplift is offset to the NW with respect to the geometric crater center. It should be noted that, although part of the faults curvature in the map is a topographic effect, the strong bends in the faults lying NE and SW of the center are related to late-stage bending and rotation of the foot wall rocks and faults out of a radial orientation.

4.2. Breached uplift

Within the center, the two aforementioned sectors are separated by a large SE-trending reverse fault, along which top-to-the NE thrusting occurred (Fig. 2A). Though strongly modified by radial faulting, the strata in the northeastern sector form a broken anticline that

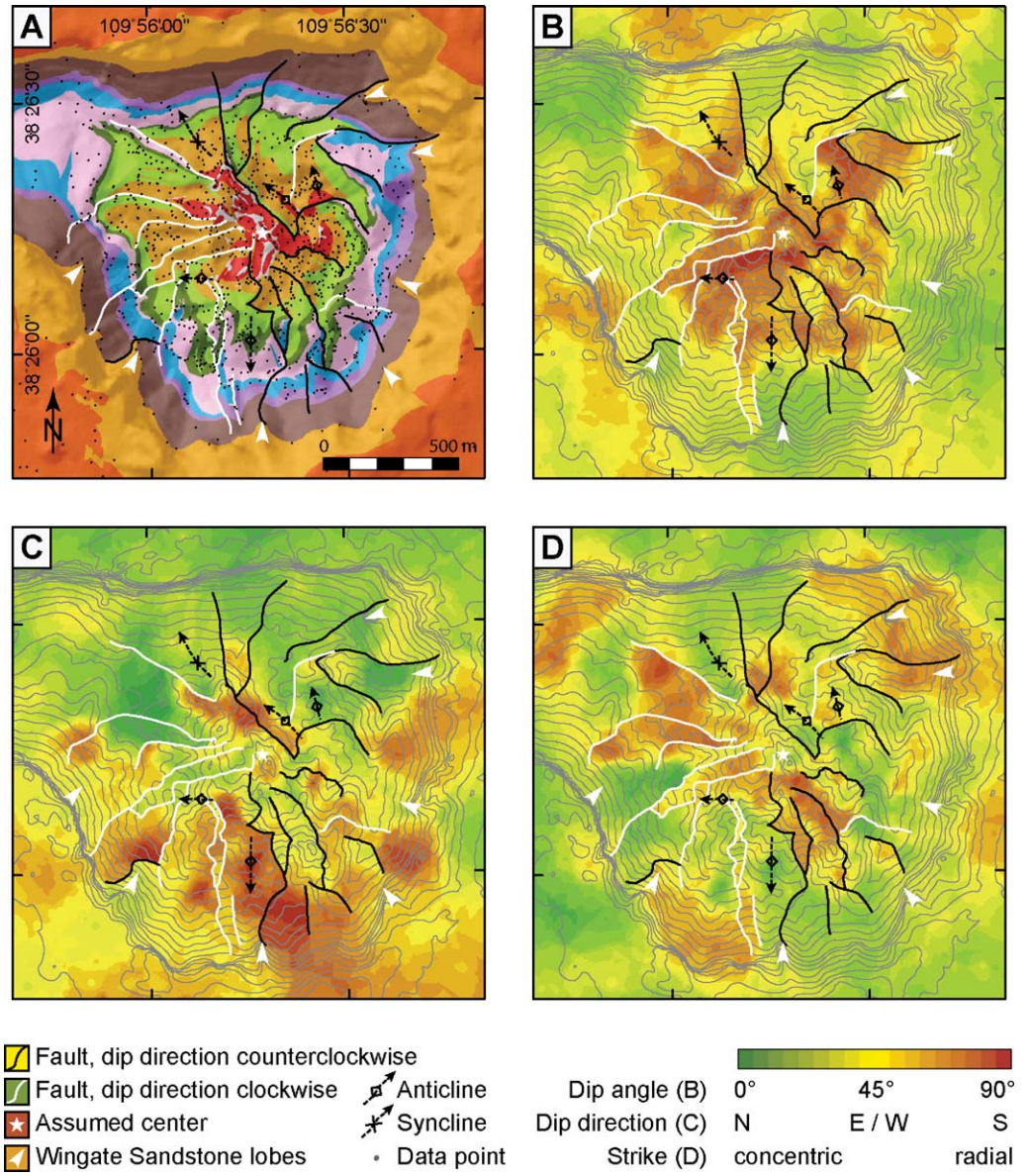

Fig. 3. Maps from the innermost part of the central uplift that show the strata orientation. Major radial faults distinguished by their direction of dip with respect to the center (white star). (A) Geological overview with data points. (B) Dip angles. (C) Dip direction, not distinguishing between E and W, thus depicting a shaded structure map, with the source of illumination from N. (D) Strike of strata with respect to the center. Thematic maps (B–D) generated by inverse distance weighted interpolation, using 8 neighboring data points and a power of 0.5 to smooth the surface, as well as the shown faults as sampling barriers for separating individual tectonic blocks. Calculations based on a compilation of about 1200 data points, collected during our own field study and derived from the geological map by [28].

trends parallel (SE) to the central reverse fault and displays opposing plunges at its ends. In the hanging wall of the central reverse fault, rocks of the lowermost outcropping unit, the White Rim Sandstone, are roughly aligned from the syncline in the NW across the center to the anticline in the S. Remnants of lower Ali Baba rocks and the distribution of White Rim and Hoskinnini rocks, indicate that the strata likewise formed an anticline that got dissected by radial faults. Thus, the center of Upheaval Dome is marked by two roughly SE-trending structural highs, of which the southwestern has been thrusted upon the northeastern.

4.3. Patterns of strata orientation

Fig. 3 shows three thematic maps that have been generated by interpolating the bedding orientation across the innermost part of the central uplift using the

major radial faults as sampling boundaries. Although the resulting patterns are complicated by lateral differences in topographic height, and therefore exposure depth, and the aforementioned uneven division of the central part by the SE-trending fault, some bilateral symmetry across an axis trending NW–SE appears to characterize the orientation of the strata. Dip angles (Fig. 3B) generally increase towards the center. Equidistant to the center, strata from a deeper level show relatively lower dip angles, as seen in the N and W. However, the northwestern sector displays some steeply dipping strata close to the aforementioned syncline, the bounding faults of which show exceptionally large throws near the center (see Fig. 2B). This reflects large magnitudes of thrusting and upward-rotation of the strata in this sector, which is supported by its structural elevation. A large amount of top-to-the SE-directed thrusting and rotation of rocks is further marked by overturned strata in between the syncline and the center, as shown in Fig. 3C, which depicts the dip direction of the strata. Moving in towards the center, the strike of the strata is generally grading from concentric to radial orientation with respect to the center, which reflects increasing concentric shortening and hence rotation of the thrust slices. However, Fig. 3D, which displays the strike pattern, shows marked deviations from axial symmetry, and rather displays bilateral symmetry across a NW–SE-trending symmetry axis. Radial striking strata is clearest developed adjacent to the syncline and in an area extending SE from the center towards a pop-up structure. Flanking this southeastern sector are domains with dominantly concentrically oriented strata. At larger distances from the center, radial striking strata can be observed in the northeastern and south–southwestern corner of the central topographic depression and is associated with radial faults that extend up to the Wingate Sandstone unit where they accommodated unusual large (>50 m) displacements. In both cases, the SE-directed transport was accompanied by bending and rotating the faults and strata of the foot wall around a hinge zone approximately marked by steeply plunging folds (Fig. 2A). This late-stage rotation and bending rearranged the strata further inward into more concentric strikes and most likely formed the radial striking domain in the SE and the associated pop-up by lateral confinement. Therefore, the strata orientation documents amplified NW–SE shortening at the syncline in the northwestern sector and in the northeastern and southwestern sectors of the central topographic depression.

4.4. Magnitude of concentric shortening of Wingate Sandstone

The circumferential trace of the Wingate–Church Rock contact (Fig. 2A) gives an estimate of the amount of radial folding and thus concentric shortening at a somewhat higher level. The sites of strongest undulations are marked by the occurrence of lobate-shaped bodies of Wingate Sandstone that reach into the underlying Chinle Formation (Fig. 2A, and indicated by arrowheads in Fig. 3). These features and associated clastic dikes are inferred to be the product of increased internal strain accumulation and disintegration by microfaulting during concentric shortening and subsequent granular and cataclastic flow (cf. [17]). In the

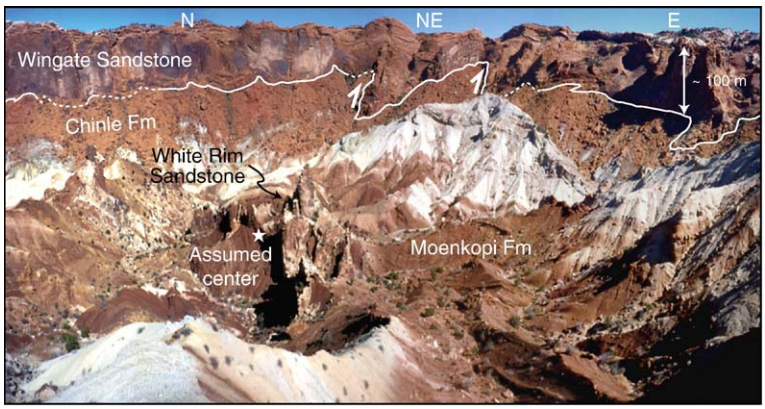

Fig. 4. Panoramic image of the northern to eastern perimeter of the central topographic depression. Radial folds in the Wingate Sandstone are visible as undulations in the trace of the Wingate-Chinle contact. The contact is dashed where covered by talus. Radial reverse faults in the northeastern corner show large displacements and make their way exceptionally high into the Wingate Sandstone. Note the centrally located dikes of White Rim Sandstone, surrounded by rocks from the Moenkopi Formation. The well visible transition from dark- to bright-colored rocks marks the contact of the upper and lower Ali Baba member in the Moenkopi Formation.

northeastern and southwestern corners, the largest undulations and sandstone lobes are clearly linked to radial faults that have climbed into the Wingate unit, forming fault-propagation folds (Fig. 4). These sandstone lobes can also be found in the southeastern sector, but are generally smaller and lack well-developed radial faults. Along the northern perimeter of the central topographic depression, however, undulations of the contact are small and sandstone lobes are lacking (Fig. 4), even though the Wingate outcrops are equally or less distant from the center compared to the other sectors. This points to a smaller amount of concentric shortening in the N and possibly NW, due to less convergence during inward movement. Decreased concentric shortening could also be accounted for by a smaller amount of inward movement, but that contradicts the aforementioned support for amplified SE-directed thrusting in the northwestern part of the central topographic depression (see patterns of strata orientation).

4.5. Decreasing asymmetry outwards

Although our field mapping comprised only the central topographic depression, we were able to trace the layering of the Kayenta Formation that provides information of its large-scale straining, by using high-resolution aerial and satellite images. Delineated by wavy black lines in Fig. 1, the bedding traces can be seen to depart from an idealized circular arrangement around the center. Within the individual bedding traces, the short wavelength curvatures, i.e. tens to a hundred meters, are the result of intraformational deformation as well as topography. However, the large-scale trend of the bedding traces taken together, roughly define the outline of an ellipse (white lines), with the long axis trending NE–SW, and an aspect ratio of ~1.1. The center of this best-fit ellipse is displaced by 50–100 m to the SE of the assumed center, the location of which is supported by the distance to the ring syncline and rim monocline (see below). The sectors of strongest curvature are located in the NE and SW, i.e. above the radial faults with large SE-directed displacements (cf. Fig. 2A). The beds at the east–southeastern edge of the central topographic depression display an even lower curvature than the ellipse suggests. Departure from the elliptical shape near the canyon in the WNW and on a ridge in the SSE is due to topographic lows and highs, respectively. Since the height of the outcropping Kayenta Formation is otherwise very similar, we use this ellipse as a strain marker and infer an overall increased shortening in the NW–SE direction, which conforms to the data presented above.

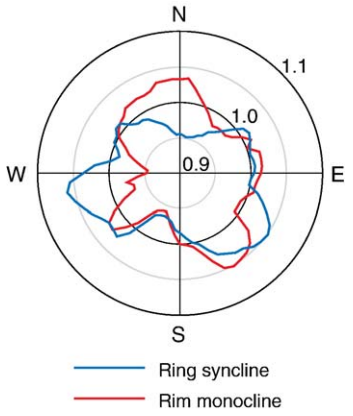

Fig. 5. Pole diagram that depicts the distance of the ring syncline and rim monocline from the center of Upheaval Dome, normalized by the average distance, 1806 m and 2586 m, respectively.

At greater distances from the center, however, the asymmetry of the central uplift decreases, as our examination of the shape of the ring syncline and the rim monocline shows. The traces of both features are given by [28,29], who presented slightly differing results. For our measurements, we first corrected for any jumps in distance from the center due to topographic steps and then averaged the position of both features as given by the two author teams (Fig. 1). The distance of the syncline and monocline axis from the center was measured at 5° steps and normalized by the average distance. The results in Fig. 5 do not show a systematic elongation in a certain direction. While both features are elongated somewhat to the SE, the syncline extends to the N and a little to the SW, and the monocline extends further out in the W and is less far from the average in the N. However, the standard deviations from the mean are merely 53 and 67 m for the syncline and monocline, respectively, which is, especially for the often hard to reach syncline, within mapping inaccuracy.

5. Discussion

In summary, the presented arguments indicate that the lateral displacement field included a SE-directed component in addition to the overall centripetal movement during crater collapse. This resulted in enhanced shortening in the NW–SE direction. We argue that this can be attributed to the impact direction rather than to anisotropies of the target. The slight 1° inclination of the target rocks towards the NNW roughly

coincides with the proposed impact direction. However, assuming that not the impact direction but only the targets properties influenced the kinematics of central uplift formation, we would expect favored thrusting in the dip direction, i.e. top to the NNW. This expectation relies on the observation that bedding planes are often sites of strain localization [17,26], and thus offer less frictional resistance in a down sloping direction. Furthermore, we can think of no mechanism that relates the observed kinematical asymmetry to the regional sub-vertical joint set (most joints trending 130° and 160° and some 105°), which largely postdates the impact event [17].

For the impact angle to influence the kinematics of crater collapse, it is required that the horizontal momentum component of an obliquely striking projectile is transferred to the target and can be traced until the beginning of crater collapse. Dahl and Schultz [31] found in an experimental cratering study in aluminum that, during oblique impact-induced stress wave passage, the momentum content per unit area of the stress wave within the target is largest in the downrange direction. Furthermore, using high-resolution optical monitoring of experimental impacts into sand, Anderson et al. [32] observed that, at impact angles of less than 45°, the sub-surface flow field center appeared to migrate downrange during the excavation of the transient cavity to half its final size. However, during growth of the (simple) crater to its final diameter, this migration ceased. Yet, in numerical studies of impact crater collapse, it is often observed that the floor of the transient cavity begins to rise, while its diameter is still increasing, i.e. the transient cavity is still being excavated [20,33,34]. Specifically, Shuvalov [23] modeled the formation of complex craters by asteroids of 0.5 km and 8 km diameter striking their target from 90° to 30°. In the oblique cases, he observed that the uprange region of the transient cavity floor reached its maximum depth, while the downrange region still moved outward, and that the rising crater floor is subsequently offset uprange (cf. [24]). A similar observation can be found in Fig. 4 of [34], who modeled the formation of a Chicxulub-scale crater by an oblique impact. Therefore, we propose that the horizontal momentum component of an obliquely striking projectile is preserved until the onset of crater collapse and will be recorded in the core of the central uplift. More precisely, the start of crater collapse and central uplift formation uprange and its downrange propagation with time, result in the formation of systematically imbricated slices and enhanced shortening within the impact direction. However, at later stages, the downrange migration of the rising central uplift obscures any morphological asymmetries [23,24], which are, therefore, lacking in crater morphometric studies [21]. This is also supported by our observations at Upheaval Dome, where the structural asymmetries are largest in the core of the central uplift and decrease outwards, thereby preserving the large-scale circular shape of the main structural elements, i.e. rim monocline and ring syncline. The reason for the waning asymmetry during central uplift formation is the early onset as well as cease of centripetal movement in the roots of the central uplift compared to the more distal regions. Therefore, the development of structural asymmetries at shallow levels in the central uplift or the crater rim area may be confined to extremely low impact angles.

Amongst the asymmetric structures at Upheaval Dome, the prominent fault arrangement in the innermost part of the central uplift appears to be suited as a general criterion for the identification of an asymmetric flow field during crater collapse and hence the impact direction. However, identification may be limited to craters, where marker horizons, e.g. layered sedimentary rocks, permit to evaluate the relative motion of the fault blocks or slices and the dominant thrusting direction. Fig. 6 shows simplified sketches from the innermost part of the central uplifts of (A) Upheaval Dome, as well as the (B) Spider, $D \sim 12$ km [15], and (C) Gosses Bluff impact structures, $D \sim 24$ km [35]. The Spider and Gosses Bluff craters are also developed in weakly deformed sedimentary rocks. They display a very similar arrangement of aligned imbricated fault blocks as seen at Upheaval Dome. The consistency of SSE (Spider)- and SSW (Gosses Bluff)-directed thrusting is even more striking than at Upheaval Dome. We suspect that the thrust direction in these cases also reflects a prevailing lateral displacement direction during crater collapse, and thus and oblique impact as indicated by the arrow heads (see Fig. 6, cf. [15]).

Amongst the structural criteria for oblique impacts proposed by Schultz and Anderson [14], an uprange offset of the central uplift with regard to the final crater center can be observed at the lowermost outcropping units at Upheaval Dome, i.e. Permian White Rim Sandstone and Triassic Moenkopi Formation, but is not evident in the Jurassic Kayenta Formation. At Gosses Bluff, no uprange offset of the central uplift is evident on the basis of geophysical data [36], and for Spider, an uprange offset is possible, but difficult to judge on the basis of the existing geological data [15,37].

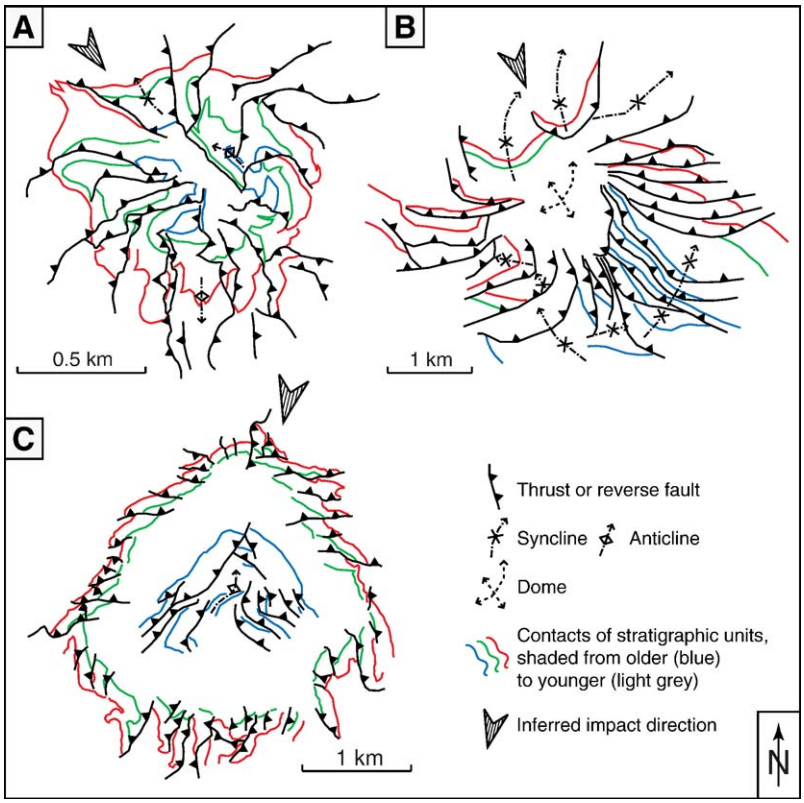

Fig. 6. Simplified sketches of faults and contacts from the innermost part of the central uplifts of eroded complex craters in sedimentary target rocks: (A) Upheaval Dome, United States, $D \sim 5.3$ km; (B) Spider, Australia, $D \sim 12$ km, after [15]; (C) Gosses Bluff, Australia, $D \sim 24$ km, after [35].

Furthermore, the proposed large central uplift diameter compared to final diameter [14] is a characteristic of the presently exposed level of Upheaval Dome (~ 1.43), but not known at Spider and Gosses Bluff, due to alluvial cover. A breaching of the central uplift can be observed at Upheaval Dome, but there is no obvious alignment in the downrange direction as proposed by [14]. However, in the innermost part of Gosses Bluff, the central uplift is breached in the proposed downrange direction. It should be noted, though, that the cited examples are structural features, whereas the most prominent example of a breached uplift, i.e. Lunar King crater, is a morphological one [14]. Finally, we do not know if an enhanced rim/wall collapse in the uprange direction occurred at any of the structures, but such a feature would be consistent with the model of an uprange initiation and downrange migration of the rising central uplift. In summary, of the discussed criteria diagnostic of oblique impacts, a consistent thrust direction may be the most useful criterion in the study of eroded complex craters in layered sedimentary target rocks. Additionally and in contrast to the breached central uplift criterion, it is based on a kinematical model supported by numerical studies.

6. Conclusions

The analysis of the internal structural geometry of the central uplift at the Upheaval Dome impact structure suggests a systematic departure from a pure axial symmetric flow field during crater collapse and central uplift formation. Enhanced shortening roughly in the NW–SE direction is most evident in the core of the central uplift, where a set of imbricated slices displays top to the SE thrusting. Further outward and upward the structural asymmetry is preserved in dominant radial faults and an elliptical bedding outline but disappears at the edge of the central uplift, i.e. the ring syncline. With regard to experimental and numerical studies of oblique impact cratering, we infer that this lateral displacement component reflects a shift in the onset of crater collapse and the migration of the uplifting crater floor downrange, i.e. in the impact direction. The remarkable consistent arrangement of imbricate slices in the core of the central uplift

can also be found in the Australian Spider and Gosses Bluff impact structures and may provide a diagnostic tool for identification of the impact direction in deeply eroded complex craters that were formed in sedimentary targets by an oblique impact.

Acknowledgements

This work was funded by the Deutsche Forschungsgemeinschaft (DFG) grant KE-732/6-1. We are grateful to the United States Department of the Interior National Park Service for providing scientific research permits. The manuscript benefited from a constructive review by Gordon Osinski and the editor Richard W. Carlson.

References

[1] B.M. French, The importance of being cratered: the new role of meteorite impact as a normal geological process, Meteorit. Planet. Sci. 39 (2) (2004) 169–197.
[2] E.M. Shoemaker, Interpretation of lunar craters, in: Z. Kopal (Ed.), Physics and Astronomy of the Moon, Academic Press, New York, 1962, pp. 283–351.
[3] E. Pierazzo, H.J. Melosh, Understanding oblique impacts from experiments, observations, and modeling, Annu. Rev. Earth Planet. Sci. 28 (2000) 141–167.
[4] D. Gault, J.A. Wedekind, Experimental studies of oblique impacts, Proc. Lunar Planet. Sci. Conf. 9 (1978) 3843–3875.
[5] W.F. Bottke Jr., S.G. Love, D. Tytell, T. Glotch, Interpreting the elliptical crater populations on Mars, Venus, and the Moon, Icarus 145 (2000) 108–121.
[6] R.R. Herrick, N.K. Forsberg-Taylor, The shape and appearance of craters formed by oblique impact on the Moon and Venus, Meteorit. Planet. Sci. 38 (11) (2003) 1551–1578.
[7] J.M. Dahl, P.H. Schultz, Shock decay in oblique impacts, Lunar Planet. Sci. Conf. 29 (1998) (Contribution #1958).
[8] E. Pierazzo, H.J. Melosh, Hydrocode modeling of Chicxulub as an oblique impact event, Earth Planet. Sci. Lett. 165 (1999) 163–176.
[9] P.H. Schultz, S. D'Hondt, Cretaceous–Tertiary (Chicxulub) impact angle and its consequences, Geology 24 (1) (1996) 963–967.
[10] A.R. Hildebrand, M. Pilkington, J. Halpenny, R. Cooper, M. Connors, C. Ortiz-Aleman, R.E. Chavez, J. Urrutia-Fucugauchi, E. Graniel-Castro, A. Camara-Zi, R.T. Buffler, Mapping Chicxulub crater structure with overlapping gravity and seismic surveys, Lunar Planet. Sci. Conf. 29 (1998) (Contribution #1821).
[11] L.E. Nyquist, Do oblique impacts produce Martian meteorites? LPSC 13 (1982) 602–603.
[12] J.D. O'Keefe, T.J. Ahrens, Oblique impact—a process for obtaining meteorite samples from other planets, Science 234 (1986) 346–349.
[13] N.A. Artemieva, B.A. Ivanov, Launch of Martian meteorites in oblique impacts, Icarus 171 (2004) 84–101.
[14] P.H. Schultz, R.R. Anderson, Asymmetry of the Manson impact structure: evidence for impact angle and direction, Spec. Pap.-Geol. Soc. Am. 302 (1996) 397–417.
[15] E.M. Shoemaker, C.S. Shoemaker, The proterozoic impact record of Australia, AGSO J. Aust. Geol. Geophys. 16 (4) (1996) 379–398.
[16] D. Stöffler, N.A. Artemieva, E. Pierazzo, Modeling the Ries-Steinheim impact event and the moldavite strewn field, Meteorit. Planet. Sci. 37 (2002) 1893–1907.
[17] T. Kenkmann, A. Jahn, D. Scherler, B.A. Ivanov, Structure and formation of a central uplift: a case study at the Upheaval Dome impact crater, Utah, Spec. Pap.-Geol. Soc. Am. 384 (2005) 85–115.
[18] F. Tsikalas, Mjölnir crater as a result of oblique impact: asymmetry evidence constrains impact direction and angle, in: C. Koeberl, H. Henkel (Eds.), Impact Tectonics, Springer Verlag, Berlin, 2005, pp. 285–306.
[19] M. Lindström, V.V. Shuvalov, B.A. Ivanov, Lockne crater as a result of marine-target oblique impact, Planet. Space Sci. 53 (2005) 803–815.
[20] H.J. Melosh, Impact Cratering—A Geologic Process, Oxford University Press, New York, 1989, 245 pp.
[21] A.G. Ekholm, H.J. Melosh, Crater features diagnostic of oblique impacts: the size and position of the central peak, Geophys. Res. Lett. 28 (4) (2001) 623–626.
[22] P.H. Schultz, Effect of impact angle on central-peak/peak-ring formation and crater collapse on Venus, Lunar Planet. Sci. Conf. 23 (1992) (Contribution #789).
[23] V.V. Shuvalov, Cratering process after oblique impacts, Third International Conference on Large Meteorite Impacts, Nördlingen, 2003, Contribution #4130.
[24] V.V. Shuvalov, H. Dypvik, Ejecta formation and crater development of the Mjölnir impact, Meteorit. Planet. Sci. 39 (3) (2004) 467–479.
[25] P.W. Huntoon, G. H. Billingsley Jr., W.J. Breed, Geologic map of Canyonlands National Park and vicinity, Utah, 1:62 500, The Canyonlands Natural History Association, Moab, 1982.
[26] E.M. Shoemaker, K.E. Herkenhoff, Upheaval Dome impact structure, Utah, Lunar Planet. Sci. Conf. 15 (1984) 778–779.
[27] T. Kenkmann, I. von Dalwigk, Radial transpression ridges: a new structural feature of complex impact craters, Meteorit. Planet. Sci. 35 (2000) 1189–1201.
[28] B.J. Kriens, E.M. Shoemaker, K.E. Herkenhoff, Geology of the Upheaval Dome impact structure, southeast Utah, J. Geophys. Res. 104 (E8) (1999) 18867–18887.
[29] M.P.A. Jackson, D.D. Schultz-Ela, M.R. Hudec, I.A. Watson, M. L. Porter, Structure and evolution of Upheaval Dome: a pinched off salt diapir, Geol. Soc. Amer. Bull. 110 (12) (1998) 1547–1573.
[30] T. Kenkmann, Dike formation, cataclastic flow, and rock fluidization during impact cratering: an example from the Upheaval Dome structure, Utah, Earth Planet. Sci. Lett. 214 (2003) 43–58.
[31] J.M. Dahl, P.H. Schultz, In-target stress wave momentum content in oblique impacts, Lunar Planet. Sci. Conf. 30 (1999) (Contribution #1854).
[32] J.L.B. Anderson, P.H. Schultz, J.T. Heineck, Experimental ejection angles for oblique impacts: implications for the subsurface flow-field, Meteorit. Planet. Sci. 39 (2) (2004) 303–320.
[33] H.J. Melosh, B.A. Ivanov, Impact crater collapse, Annu. Rev. Earth Planet. Sci. 27 (1999) 385–415.
[34] B.A. Ivanov, N.A. Artemieva, Numerical modeling of the formation of large impact craters, Spec. Pap.-Geol. Soc. Am. 356 (2002) 619–630.

[35] D.J. Milton, A.Y. Glikson, R. Brett, Gosses Bluff—a latest Jurassic impact structure, central Australia: Part 1. Geological structure, stratigraphy, and origin, AGSO J. Aust. Geol. Geophys. 16 (4) (1996) 453–486.
[36] D.J. Milton, B.C. Barlow, A.R. Brown, F.J. Moss, E.A. Manwaring, E.C.E. Sedmik, G.A. Young, J. Van Son, Gosses Bluff—a latest Jurassic impact structure, central Australia: Part 2. Seismic, magnetic, and gravity studies, AGSO J. Aust. Geol. Geophys. 16 (4) (1996) 487–527.
[37] A. Abels, Spider impact structure, Kimberley Plateau, western Australia: interpretations of formation mechanism and age based on integrated map-scale data, Aust. J. Earth Sci. 52 (2005) 653–664.